

Unambiguous optimization of effective potentials in finite basis sets

Christoph R. Jacob^{a)}

Karlsruhe Institute of Technology (KIT), Center for Functional Nanostructures,
Wolfgang-Gaede-Str. 1a, 76131 Karlsruhe, Germany

(Received 22 May 2011; accepted 28 November 2011; published online 23 December 2011)

The optimization of effective potentials is of interest in density-functional theory (DFT) in two closely related contexts. First, the evaluation of the functional derivative of orbital-dependent exchange-correlation functionals requires the application of optimized effective potential methods. Second, the optimization of the effective local potential that yields a given electron density is important both for the development of improved approximate functionals and for the practical application of embedding schemes based on DFT. However, in all cases this optimization turns into an ill-posed problem if a finite basis set is introduced for the Kohn–Sham orbitals. So far, this problem has not been solved satisfactorily. Here, a new approach to overcome the ill-posed nature of such finite-basis set methods is presented for the optimization of the effective local potential that yields a given electron density. This new scheme can be applied with orbital basis sets of reasonable size and makes it possible to vary the basis sets for the orbitals and for the potential independently, while providing an unambiguous potential that systematically approaches the numerical reference.

© 2011 American Institute of Physics. [doi:10.1063/1.3670414]

I. INTRODUCTION

Kohn–Sham density functional theory (KS-DFT)^{1,2} is arguably the most successful method for electronic structure calculations. Even though it is a formally exact theory, KS-DFT relies on approximations for the exchange-correlation (xc) energy functional $E_{xc}[\rho]$ or its functional derivative, the xc potential $v_{xc}[\rho](\mathbf{r}) = \delta E_{xc}[\rho]/\delta\rho(\mathbf{r})$. These density functional approximations (DFAs) can be classified according to rungs on “Jacob’s ladder”.³ Most of the success of DFT stems from the fact that often a good accuracy can already be achieved at the two lowest rungs—the local density approximation (LDA) and generalized-gradient approximations (GGA), i.e., explicit DFAs depending on the local electron density only or on the local electron density and its gradient, respectively.

However, the limitations of LDA and GGA (e.g., dramatic failures when stretching bonds in molecules, for predicting spin-state energies in transition metal compounds, or for calculating band gaps in solids) have also become clear.⁴ Therefore, next-generation DFAs, occupying higher rungs on “Jacob’s ladder,” are being developed (see, e.g., Refs. 5–8). Such DFAs take, in addition to the local electron density and its gradient, also the kinetic-energy density, occupied KS orbitals, and virtual KS orbitals into account. Therefore, they do not depend explicitly on the electron density, but instead constitute implicit density functionals, as the KS orbitals implicitly depend on the electron density.

For orbital-dependent xc-functionals, the corresponding xc potential $v_{xc}(\mathbf{r})$ cannot be determined directly as the explicit functional derivative of $E_{xc}[\rho]$. Instead, the optimized effective potential (OEP) method⁹ is usually applied, in which the xc potential is determined by searching for the local

potential yielding those orbitals that minimize the orbital-dependent total energy functional. This leads to an integral equation for the xc potential. By expanding the xc potential in a finite basis set, this OEP integral equation can either be solved by a self-consistent scheme¹⁰ or through a direct optimization.^{11,12}

For calculations on many-electron systems to be feasible, a finite basis set expansion is commonly employed for the KS orbitals. With LDA and GGA xc functional, basis sets of relatively small size (split-valence up to triple-zeta quality) are usually sufficiently accurate, which makes DFT calculations on large molecular systems possible.^{13,14} Unfortunately, it turns out that with such finite orbital basis sets, the OEP problem is ill-posed and the xc potential is no longer uniquely defined. As a consequence, one can obtain highly oscillatory and thus unphysical xc potentials.^{15,16} This significantly affects orbital-energy differences, which in turn determine spectroscopic properties and might also enter the xc functional. If the xc potential is not unique, the resulting orbitals, spectroscopic properties, and possibly also the energies will be ambiguous.

These problems present significant obstacles for routine application of the OEP method and thus hamper the development of next-generation orbital-dependent xc functionals. One practical solution is to carefully choose the orbital and potential basis sets to be “balanced”.¹⁷ However, this is often difficult to achieve and requires the use of very large orbital basis sets. Therefore, such an approach is only feasible for benchmark calculations on small molecules, and becomes impossible for larger molecular systems. Another approach has been developed by Yang and co-workers,^{16,18} who suggest to change the energy functional such that it includes a smoothness measure. This way it is ensured that the resulting potentials are as smooth as possible. However, it is not clear whether such a smooth potential is actually the

^{a)}Electronic mail: christoph.jacob@kit.edu.

physically desired solution. Thus, better approaches to the OEP problem are necessary. Such an improved OEP scheme should (a) yield an unambiguous potential that is not sensitive to the initial guess or parameters of the numerical algorithm, (b) be applicable for any combination of orbital and potential basis sets and thus allow one to systematically enlarge the potential basis set for any given orbital basis set, including orbital basis sets of reasonable size, and (c) result in a potential that approaches the exact numerical OEP solution in the limit of large orbital and potential basis sets. Ideally, the convergence with the size of the orbital basis set should be fast to allow for the use of orbital basis sets of reasonable size in practical calculations.

For developing such an OEP scheme, instead of KS-DFT calculations with orbital-dependent functionals, a closely related but conceptually simpler problem is considered here: the reconstruction of the local potential yielding a given target electron density. This is equivalent to evaluating the functional derivative of the (orbital-dependent) noninteracting kinetic-energy functional $T_s[\{\phi_i\}]$. Therefore, the reconstruction of local potentials from electron densities can be achieved with numerical schemes^{19,20} that are often closely related to the OEP methods discussed above.¹² However, as soon as a finite orbital basis set is introduced, they suffer from the same numerical problems as these OEP methods, and result in ambiguous and often unphysical potentials.

Because of this close relation between the OEP and the potential reconstruction problem, progress made for the latter problem for overcoming the numerical difficulties resulting from its ill-posed nature will open the way towards improved OEP schemes. Moreover, the reconstruction of the local potential yielding a given electron density is also of interest by itself. By using electron densities from highly accurate calculations, it can be used to obtain accurate xc potentials that can serve as guidance for constructing DFAs.^{20–23} Recently, this has for instance been employed to study accurate adiabatic connection curves.^{24–27} Furthermore, the functional derivative of the non-interacting kinetic energy is of central importance in DFT-based embedding schemes and in subsystem-DFT methods.^{28,29} By reconstructing the local potential that yields a given density, it is possible to assess the approximations used in such schemes^{30,31} and to develop accurate subsystem-DFT approaches³² as well as embedding methods combining different quantum-chemical levels of accuracy.^{33–35} However, all these applications possibly suffer from the numerical problems of the existing methods for the optimization of effective potentials in finite basis sets.

This work is organized as follows. In Sec. II, the theoretical background and the direct optimization algorithm by Wu and Yang,^{11,12} which will serve as our starting point, are briefly reviewed. After giving the computational details in Sec. III, the ill-defined nature of the optimization of effective potentials in finite basis sets is investigated more closely in Sec. IV. In Sec. V, it is shown how it is possible to overcome this problem by singling out one optimized potential, and in Sec. VI, a condition for determining an optimal optimized potential is proposed. The new scheme is then applied to atoms and molecules in Secs. VII and VIII, respectively. Finally, conclusions are summarized in Sec. IX.

II. THEORETICAL BACKGROUND

In KS-DFT, the solution of the Schrödinger equation for a system of interacting electrons is mapped onto a reference system of non-interacting electrons.^{1,2} For this non-interacting reference system, the wavefunction is given by a single Slater determinant, with orbitals determined by solving the KS equations,

$$\left[-\frac{1}{2}\Delta + v_s(\mathbf{r}) \right] \phi_i(\mathbf{r}) = \epsilon_i \phi_i(\mathbf{r}), \quad (1)$$

where $v_s(\mathbf{r})$ is a local potential. For the exact ground-state density of a system of interacting electrons, this local potential is given by the Kohn–Sham potential,

$$v_{\text{KS}}(\mathbf{r}) = v_{\text{nuc}}(\mathbf{r}) + v_{\text{Coul}}(\mathbf{r}) + v_{\text{xc}}(\mathbf{r}), \quad (2)$$

where $v_{\text{nuc}}(\mathbf{r})$ is the nuclear potential, $v_{\text{Coul}}(\mathbf{r})$ is the Coulomb potential of the electrons and the exchange-correlation potential $v_{\text{xc}}(\mathbf{r}) = \delta E_{\text{xc}}/\delta\rho(\mathbf{r})$ is given by the functional derivative of the exchange-correlation energy. However, for any local potential $v_s(\mathbf{r})$, the electron density $\rho_0(\mathbf{r})$ obtained from solving the KS equations fulfills the Euler-Lagrange equation,²

$$\left. \frac{\delta T_s[\rho]}{\delta\rho} \right|_{\rho=\rho(\mathbf{r})} + v_s(\mathbf{r}) = \mu, \quad (3)$$

where $T_s[\rho] = \sum_i \langle \phi_i | -1/2\Delta | \phi_i \rangle$ is the functional of the kinetic energy of the non-interacting reference system. Therefore, for the density $\rho_0(\mathbf{r})$ the functional derivative of $T_s[\rho]$ is given by the negative of the local potential $v_s(\mathbf{r})$ that yields this density,³⁶ plus a constant shift given by the chemical potential μ . To evaluate this functional derivative for a given target density $\rho_0(\mathbf{r})$ is thus equivalent to determining the local potential that has this density as its ground state.

Several methods for reconstructing the local potential yielding a given target density have been developed.^{19–21,37,38} Here, we will consider the direct optimization method of Wu and Yang (WY),^{11,12} which is conceptually rather straightforward and can be easily extended to the evaluation of other orbital-dependent functionals.^{12,39} As shown in Ref. 12, the local potential yielding the target density $\rho_0(\mathbf{r})$ can be determined by maximizing the Lagrangian,

$$W_s[v_s] = -\frac{1}{2} \sum_i \langle \phi_i | \Delta | \phi_i \rangle + \int v_s(\mathbf{r})(\rho(\mathbf{r}) - \rho_0(\mathbf{r})) d^3r, \quad (4)$$

with respect to the potential $v_s(\mathbf{r})$, where $\phi_i(\mathbf{r})$ and $\rho(\mathbf{r})$ are the occupied KS orbitals and the density obtained from this potential, respectively. The total potential $v_s(\mathbf{r})$ can then be expanded as

$$\begin{aligned} v_s(\mathbf{r}) &= v_{\text{nuc}}(\mathbf{r}) + v_{\text{Coul}}(\mathbf{r}) + v_{\text{xc}}(\mathbf{r}) \\ &= v_{\text{nuc}}(\mathbf{r}) + v_{\text{Coul}}(\mathbf{r}) + v_0(\mathbf{r}) + \sum_t b_t g_t(\mathbf{r}), \end{aligned} \quad (5)$$

where $v_0(\mathbf{r})$ is an initial guess for the exchange-correlation potential and $\{g_t(\mathbf{r})\}$ is a basis set for the potential. Note that the last two terms, $v_0(\mathbf{r})$ and the part expanded in basis functions $v_b(\mathbf{r}) = \sum_t b_t g_t(\mathbf{r})$, correspond to the xc potential $v_{\text{xc}}(\mathbf{r})$. With this expansion, the problem turns into a maximization with respect to the coefficients $\{b_t\}$. The first and

second derivatives of the Lagrangian with respect to these coefficients can be calculated analytically as

$$\frac{\partial W_s}{\partial b_t} = \int (\rho(\mathbf{r}) - \rho_0(\mathbf{r})) g_t(\mathbf{r}) d^3r, \quad (6)$$

and (assuming real orbitals)

$$\frac{\partial^2 W_s}{\partial b_t \partial b_u} = 4 \sum_{ia} \frac{\langle \phi_i | g_u | \phi_a \rangle \langle \phi_a | g_t | \phi_i \rangle}{\epsilon_i - \epsilon_a}. \quad (7)$$

Here and in the following, the common convention is used that indices i, j, \dots run over all occupied orbitals and indices a, b, \dots run over all virtual orbitals, whereas the indices s, t, u, \dots are used for the basis set expansion of the potential. The potential can then be optimized efficiently using a standard Newton maximization.

III. COMPUTATIONAL DETAILS

All finite basis set calculations have been performed with a local version of the Amsterdam density functional (ADF) package^{40,41} in combination with the PYADF scripting framework,⁴² building on our previous implementation of the WY direct optimization scheme.³⁰ In the Newton optimization, eigenvalues smaller than 10^{-6} were ignored, and in cases where the convergence was otherwise problematic a small eigenvalue shifting between 10^{-4} and 0.01 was applied. To measure the agreement between a density $\rho(\mathbf{r})$ and the target density $\rho_0(\mathbf{r})$, the absolute error in the density defined as

$$e_{\text{dens}} = \int |\Delta\rho(\mathbf{r})| d^3r, \quad (8)$$

with $\Delta\rho(\mathbf{r}) = \rho(\mathbf{r}) - \rho_0(\mathbf{r})$ is employed, and the optimization is considered as converged if e_{dens} is smaller than $10^{-4} e \text{ bohr}^{-3}$.

For the orbitals, the standard DZP, TZ2P, and QZ4P basis sets from ADF's basis set library are used. For expanding the potential, the corresponding density fitting basis sets are employed if not stated otherwise. In the case of the QZ4P-fit potential basis set, these are augmented with additional tight 1s functions. In the calculations on atoms, the initial guess for the exchange-correlation potential $v_0(\mathbf{r})$ is chosen as

$$v_0(\mathbf{r}) = -\text{erf}(r) \frac{\zeta}{|\mathbf{r}|}, \quad (9)$$

where ζ is the exponent of the most diffuse Slater function in the orbital basis set. In the molecular calculations,

$$v_0(\mathbf{r}) = -\frac{\zeta}{N} \int \frac{\rho(\mathbf{r}')}{|\mathbf{r} - \mathbf{r}'|} d^3r', \quad (10)$$

is used as initial guess. In both cases, this initial guess ensures that the optimized potentials have the correct asymptotic form.

The numerical solution of the KS equations with a given local potential for atoms has been implemented in Python using a logarithmic radial grid as described in Refs. 43 and 44. For calculating the exact reference potentials, this numerical solver is used in combination with a modified van Leeuwen-Baerends algorithm for reconstructing a local potential.^{20,38} In each step, the potential is updated at each radial grid point

by comparing the density obtained from the current potential to the target density until $e_{\text{dens}} < 10^{-4} e \cdot \text{bohr}^{-3}$.

IV. ILL-POSED NATURE OF THE OPTIMIZATION OF EFFECTIVE POTENTIALS

As an example to illustrate the ill-posed nature of the optimization of effective potentials, we consider an argon atom and choose as target density $\rho_0(\mathbf{r})$ the density calculated with the BP86 xc functional⁴⁵ in a double- ζ plus polarization (DZP) basis set of Slater-type orbitals. This target density has been obtained from a local potential and, therefore, it is known to be v_s -representable. The exact local potential $v_s(\mathbf{r})$ that yields this target density can be determined with the algorithm of Refs. 20 and 38 in combination with a numerical solution of the KS equations. The resulting xc potential, obtained by subtracting the known nuclear and Coulomb potentials, is shown as black solid line in Fig. 1(a).

Of course, this reference potential is not identical to the exact xc potential of the argon atom, because our target electron density is not exact. Moreover, it also differs from the xc potential calculated from the target density as the functional derivative of the BP86 xc energy functional, which is shown in Fig. 1(a) as black dashed line. Only for the density obtained from a self-consistent solution in a complete (infinite) basis set, these two potentials would be equal. The exact potential shows a pronounced feature at $r \approx 0.2$, which is not present in the BP86 xc potential. Moreover, the asymptotic behavior of the two potentials at large distances from the nucleus differs (not shown in the figures, which only cover the region closer to the nucleus). The finite STO basis set enforces an exponential decay of the density, which corresponds to a potential decaying as $-\zeta/r$, where ζ is the most diffuse exponent in the STO basis. On the other hand, an exponentially decaying xc potential is obtained when the functional derivative of the BP86 xc energy functional is evaluated for this density.⁴⁶

The WY method can be applied for optimizing a local potential that yields the target density $\rho_0(\mathbf{r})$ in the finite orbital basis set. One such potential is already known and is given by the local potential that was used to obtain the target density, i.e., the xc potential calculated as the functional derivative of the BP86 xc energy functional. If this potential would be used as starting potential in the WY procedure, the optimization would terminate immediately. Therefore, only the sum of the nuclear and Coulomb potential plus an initial guess $v_0(\mathbf{r})$ (see computational details in Sec. III) is used as starting potential.

First, a small even-tempered basis set of eight 1s functions with $\zeta = 17.15, 12.0, \dots, 1.41$ is employed for the potential, whereas the DZP basis set is applied for the orbitals. The xc potential resulting from such a WY optimization is shown in Fig. 1(a) as blue dashed line. It differs from the exact reference potential (black solid line), but except for the different asymptotic form (not shown in the figure) it is rather similar to the BP86 xc potential. However, if the basis set for the potential is enlarged to the DZP-fit density fitting basis set (red solid line in Fig. 1(a)) while keeping the DZP orbital basis set, the deviations from the accurate reference potential increase and large, unphysical oscillations are introduced.

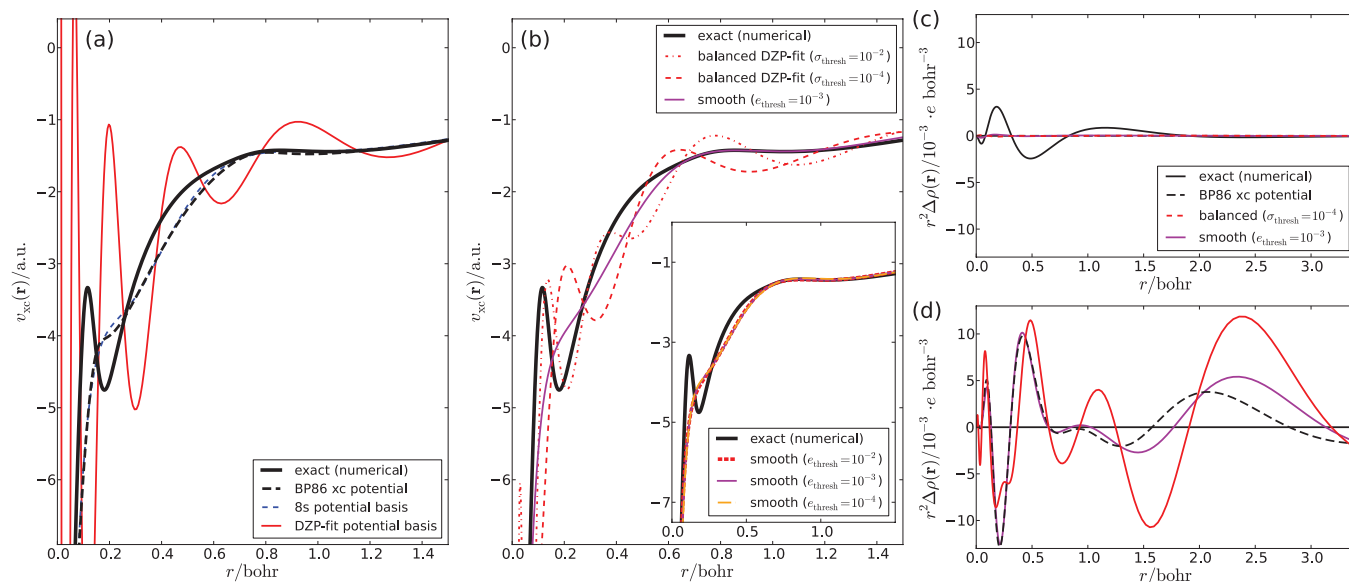


FIG. 1. (a,b): Exchange-correlation potential $v_{xc}(r)$ calculated with different schemes for optimizing the effective local potential that yields a given target density. An argon atom is considered and the BP86 ground-state density obtained in a DZP basis set is chosen as target density. See text for a detailed description of the different methods. All potentials have been shifted such that they match the exact potential at $r = 3.0$ bohr. (c,d): Radial difference $r^2 \Delta \rho(r)$ between the target density and the density obtained from the different optimized potentials (c) in the finite DZP orbital basis set and (d) when solving the KS equations numerically.

Even though the BP86 xc potential (black dashed line) and the two potentials obtained from the WY optimization (blue dashed and red solid line, respectively) differ significantly, the electron densities obtained from all three potentials within the finite DZP orbital basis set agree with the target density. The corresponding difference densities are plotted in Fig. 1(c). The density errors obtained when comparing the electron densities from these potentials to the target density are listed in Table I. Within the finite orbital basis set, the density error $e_{\text{dens}}^{\text{finite}}$ is in all three cases below the convergence threshold of $10^{-4} e \text{ bohr}^{-3}$. However, if the KS equations are solved numerically for these potentials, the electron density

deviates from the target density. The corresponding difference densities are shown in Fig. 1(d) and the density errors $e_{\text{dens}}^{\text{numerical}}$ are included in Table I. These difference densities and the corresponding density errors can be used to judge the quality of the different optimized potentials. Note, however, that for the exact potential, which reproduces the target density in such a numerical calculation, the resulting density deviates from the target density if the finite DZP basis set is applied for the orbitals (see Fig. 1(c)). We will get back to this discrepancy in Sec. VI.

These first results illustrate that if a finite orbital basis set is employed, several different potentials can yield the same electron density. Hence, the optimization of effective potentials is an ill-posed problem.^{16,47} Consequently, the WY procedure does not result in a unique potential, but its outcome often sensitively depends on the choice of the starting potential and the numerical details of the optimization algorithm.¹⁸ Moreover, if the basis set for the potential is enlarged, this problem becomes more severe and often unphysical oscillations are introduced. However, the WY optimization results in one (not necessarily unique) potential, with expansion coefficients $\{b_i^0\}$ that yields the target density within the chosen thresholds. At the same time, one obtains the occupied and virtual KS orbitals $\{\phi_i\}$ and $\{\phi_a\}$ that solve the KS equations with this potential, which are also not unique.

Nevertheless, one can now identify the reason for the non-uniqueness of the optimized potential: to first order, the change in the density caused by a change $\Delta v(r)$ of the potential is (when choosing real orbitals),

$$\Delta \rho(r) = 4 \sum_{ia} \frac{\langle \phi_i | \Delta v | \phi_a \rangle}{\epsilon_i - \epsilon_a} \phi_i(r) \phi_a(r). \quad (11)$$

Any change in the potential $\Delta v(r)$ for which $\langle \phi_i | \Delta v | \phi_a \rangle = 0$ will not mix occupied and virtual orbitals and thus leave

TABLE I. Absolute error in the electron density compared to the target density (in $e \text{ bohr}^{-1}$) obtained with the different local potentials for the argon atom with the target density from a calculation with the BP86 xc functional and a DZP basis set. The errors are given both for calculations with the finite DZP orbital basis set ($e_{\text{dens}}^{\text{finite}}$) and for a numerical solution of the KS equations ($e_{\text{dens}}^{\text{numerical}}$).

	$e_{\text{dens}}^{\text{finite}}$	$e_{\text{dens}}^{\text{numerical}}$
Exact potential	0.025	$< 10^{-4}$
BP86 xc potential	0.0	0.126
WY (8s potential basis)	$< 10^{-4}$	0.140
WY (DZP-fit potential basis)	$< 10^{-4}$	0.261
Balanced DZP-fit ($\sigma_{\text{thresh}} = 10^{-4}$)	$< 10^{-4}$	0.306
Balanced DZP-fit ($\sigma_{\text{thresh}} = 10^{-2}$)	$8.1 \cdot 10^{-4}$	0.426
Smooth ($\epsilon_{\text{thresh}} = 10^{-2}$)	$8.4 \cdot 10^{-3}$	0.172
Smooth ($\epsilon_{\text{thresh}} = 10^{-3}$)	$6.1 \cdot 10^{-4}$	0.166
Smooth ($\epsilon_{\text{thresh}} = 10^{-4}$)	$0.6 \cdot 10^{-4}$	0.147
Optimal (full)	0.051	0.026
Optimal ($\epsilon_{\text{thresh}} = 10^{-2}$)	$7.1 \cdot 10^{-3}$	0.095
Optimal ($\epsilon_{\text{thresh}} = 10^{-3}$)	$9.2 \cdot 10^{-4}$	0.122
Optimal ($\epsilon_{\text{thresh}} = 10^{-4}$)	$0.8 \cdot 10^{-4}$	0.113

the electron density unchanged. The orbital basis set is not flexible enough to “see” such changes in the potential, and, therefore, the density cannot respond to them.

However, with one (non-unique) potential and the corresponding occupied and virtual orbitals available, it is possible to identify those linear combinations of potential basis functions that can be varied without significantly changing the density. To this end, we introduce the expansion $\Delta v(\mathbf{r}) = \sum_t \Delta b_t g_t(\mathbf{r})$ with $\Delta b_t = b_t - b_t^0$ in Eq. (11), which gives

$$\Delta\rho(\mathbf{r}) = 4 \sum_t \Delta b_t \sum_{ia} \frac{\langle \phi_i | g_t | \phi_a \rangle}{\epsilon_i - \epsilon_a} \phi_i(\mathbf{r}) \phi_a(\mathbf{r}). \quad (12)$$

By further performing a singular value decomposition (SVD) $\mathbf{B} = \mathbf{U}\mathbf{\Sigma}\mathbf{V}^T$ of the matrix $B_{ia,t} = \langle \phi_i \phi_a | g_t \rangle / (\epsilon_i - \epsilon_a)$, the density change can be rewritten as

$$\begin{aligned} \Delta\rho(\mathbf{r}) &= 4 \sum_s \sigma_s \left(\sum_t V_{t,s} \Delta b_t \right) \left(\sum_{ia} U_{ia,s} \phi_i(\mathbf{r}) \phi_a(\mathbf{r}) \right) \\ &= 4 \sum_s \sigma_s \Delta \tilde{b}_s \tilde{\Phi}_s(\mathbf{r}), \end{aligned} \quad (13)$$

where σ_s are the singular values of \mathbf{B} . The right singular vectors define a transformed basis set for the potential, $\tilde{g}_s(\mathbf{r}) = \sum_t V_{t,s} g_t(\mathbf{r})$, and the corresponding change in the coefficients is $\Delta \tilde{b}_s = \sum_t V_{t,s} \Delta b_t$. Here and in the following, we use a tilde to indicate coefficients $\{\tilde{b}_t\}$ that are with respect to this transformed potential basis set. Finally, $\tilde{\Phi}_s(\mathbf{r}) = \sum_{ia} U_{ia,s} \phi_i(\mathbf{r}) \phi_a(\mathbf{r})$ are the products of occupied and virtual orbitals, transformed with the left singular vectors.

These considerations directly lead to a condition for the construction of a balanced potential basis set: as long as basis functions for the potential are within the subspace spanned by the products of occupied and virtual orbitals, so that all singular values of \mathbf{B} are different from zero, the reconstructed potential will be unique. For the small potential basis set of eight 1s functions, this is the case ($\sigma_s > 10^{-4}$), and any change to the coefficients $\{b_t\}$ will thus lead to a deterioration of the density compared to the target density. However, it is clear from Fig. 1(a) that this basis set is too small for accurately representing the exact potential, in particular the feature at $r \approx 0.2$.

For the employed DZP orbital basis set, the corresponding fit basis set for the potential is not balanced and there are 18 singular values smaller than 10^{-4} . However, a balanced potential basis set can be obtained by removing the potential basis functions \tilde{g}_t corresponding to these small singular values *a posteriori*. This is similar to the OEP scheme of Kollmar and Filatov.⁴⁸ The potential obtained with this balanced potential basis set is shown in Fig. 1(b) as red dashed line. The unphysical oscillations have now been partially removed, but the resulting potential still shows unphysical oscillations. These remain present even when a larger threshold of 10^{-2} is chosen for the singular values (red dash-dotted line in Fig. 1(b)). If these potentials are used in a numerical solution of the KS equations, the resulting density deviates significantly from the target density. The corresponding density errors in Table I are even larger than those obtained without implicitly balancing the potential basis set. The comparison of the two potentials obtained with different thresholds for the singular

values further indicate that such implicit balancing schemes are very sensitive to the choice of this threshold. Moreover, if this threshold is chosen too large, the basis set available for the potential will become too small and the density starts to deviate from the target density even within the finite orbital basis set.

Similarly, if balanced basis sets for the potential are constructed explicitly,¹⁷ it has to be chosen small enough to be contained within the space of occupied-virtual orbital products. This is often difficult to achieve, and to be able to use a reasonable basis set of the potential, very large orbital basis sets are necessary. Moreover, whether or not a given basis set for the potential is balanced will be system-dependent, as it depends on the resulting occupied and virtual orbitals. In particular, the need for very large orbital basis sets renders calculations relying on (implicitly or explicitly) balanced basis sets infeasible for larger molecules. Therefore, alternative approaches that are applicable with arbitrary orbital basis sets would be desirable.

V. SINGLING OUT ONE OPTIMIZED POTENTIAL

Instead of choosing the potential basis set small enough to be balanced, it would be preferable to be able to use arbitrary basis sets for the potential, thus allowing to approach the basis set limit for the potential with any given orbital basis. For this to be possible, additional conditions have to be found to single out one potential among those that lead—within a given threshold—to the same density. The change in the density caused by changing the coefficients in the basis set expansion of the potential by $\Delta \tilde{b}_t$ (compared to the coefficients $\{\tilde{b}_t^0\}$ obtained from the WY procedure) can be quantified by considering the absolute error in the density,

$$e_{\text{dens}} = \int |\Delta\rho(\mathbf{r})| d^3r \leq 4 \sum_t \sigma_t |\Delta \tilde{b}_t| d_t, \quad (14)$$

where $d_t = \int |\Phi_t(\mathbf{r})| d^3r$. One possibility for singling out one potential is to follow the ideas of Wang and co-workers^{16,18,49} and to determine $\{b_t\}$ such that the reconstructed part of the potential $v_b(\mathbf{r}) = \sum_t \tilde{b}_t \tilde{g}_t(\mathbf{r})$ is as smooth as possible, i.e.,

$$\int (\nabla v_b(\mathbf{r}))^2 d^3r = \int \left(\sum_t \tilde{b}_t \nabla \tilde{g}_t(\mathbf{r}) \right)^2 d^3r \rightarrow \min. \quad (15)$$

Altogether, this suggests the following algorithm. First, the WY method is used to determine one set of expansion coefficients $\{b_t^0\}$ for the reconstructed potential. These coefficients as well as the resulting occupied and virtual orbitals will in general not be unique. Next, an SVD of the matrix \mathbf{B} is calculated and the expansion coefficients are transformed with the right singular vectors, yielding the transformed coefficients $\{\tilde{b}_t^0\}$. Subsequently, a correction $\{\Delta \tilde{b}_t\}$ to the expansion coefficients is determined such that Eq. (15) is minimized, under the constraint that the right-hand side of the inequality in Eq. (14) is smaller than a threshold e_{thresh} . Such a constraint ensures that the resulting electron density still agrees with the target density, while the requirement that the potential is as smooth as possible singles out one unique potential among those yielding almost identical densities.

The unconstrained minimization of Eq. (15) is a standard quadratic optimization problem, that leads to the linear system of equations,

$$\mathbf{A}^{\text{smooth}} \Delta \tilde{\mathbf{b}} = -\mathbf{z}^{\text{smooth}}, \quad (16)$$

with $A_{st}^{\text{smooth}} = \langle \nabla \tilde{g}_s | \nabla \tilde{g}_t \rangle$ and the right-hand side $\mathbf{z}^{\text{smooth}} = \mathbf{A}^{\text{smooth}} \tilde{\mathbf{b}}_0$. With the additional inequality constraint, one has to solve a quadratic programming problem.⁵⁰ Details on the inclusion of the inequality constraint of Eq. (14) and of the implementation used here are given in Appendix A.

The algorithm described above is closely related to the scheme by Yang and co-workers,^{16,18} who include the requirement that the potential is as smooth as possible by means of an additional term in the Lagrangian. In this scheme, a parameter λ that determines the weight of this additional constraint has to be carefully chosen. If it is chosen too small, one still obtains an unphysical optimized potential, whereas with a too large λ , the resulting density starts to deviate from the target density. Moreover, in our own calculations³⁰ with the scheme of Ref. 16, we observed that the resulting potentials still sensitively depend on the choice of the starting potential and on the numerical details of the optimization procedure. The approach described above has the advantage that the threshold e_{thresh} , which determines the maximal deviation from the target density, can be chosen in advance, for instance in accordance with the convergence criterion of the WY optimization.

For the example of the argon atom considered in Sec. IV, the resulting smooth potential is shown in Fig. 1(b) as magenta line. As expected, the unphysical oscillations of the reconstructed potential are removed. Here, a threshold $e_{\text{thresh}} = 10^{-3} e \text{ bohr}^{-3}$ has been used, but almost identical potentials are obtained with $e_{\text{thresh}} = 10^{-2} e \text{ bohr}^{-3}$ and $e_{\text{thresh}} = 10^{-4} e \text{ bohr}^{-3}$. The potentials obtained with these different choices for e_{thresh} are compared in the inset in Fig. 1(b). However, it also becomes clear that requiring the reconstructed potential to be as smooth as possible is not an ideal choice. The exact reference potential shows a pronounced feature at $r \approx 0.2$, which is not recovered by the smooth reconstructed potential. Consequently, if the KS equations are solved numerically on this smooth potential, the density starts to deviate significantly from the target density, as is shown in Fig. 1(d). The corresponding absolute errors in the density, given in Table I, are smaller than for the potentials from the WY procedure without applying the smoothing constraint or with an implicit balancing scheme, but are still rather large.

VI. SINGLING OUT THE OPTIMAL OPTIMIZED POTENTIAL

Thus, for singling out one optimized potential, requiring the potential to be as smooth as possible is not a good choice and a better condition is required. Such a condition can be obtained by reconsidering the cause of the ill-posed nature of the optimization of effective potentials discussed in Sec. IV. With a finite basis set for the orbitals, the potential basis set allows for changes in the potential to which the orbitals cannot respond. However, if the orbital basis is enlarged such that it becomes sufficiently flexible, this would reveal whether these

changes in the potential cause the resulting density to deviate from the target density or not. For our example of the argon atom, this has been demonstrated here by solving the KS equations numerically with these different potentials. Both for the potentials obtained with implicitly balanced basis sets and when singling out the potential that is as smooth as possible, the density obtained in such a numerical calculation deviates significantly from the target density.

Consequently, the optimal optimized potential is the one that yields the target density even if a larger, possibly infinite, orbital basis set is used. This leads to a new scheme for singling out the optimal potential. First, the WY procedure is used to determine one non-unique potential with expansion coefficients $\{b^0\}$ that yields the target density in the finite orbital basis set. This also results in occupied orbitals $\{\phi_i\}$ that reproduce the target density. These are again not unique, but if the basis set is such that products of basis functions are not linearly dependent, which is usually the case for small to medium orbital basis sets,^{15,51} the occupied orbitals are related by a unitary transformation.

One can then determine a correction $\{\Delta b_t\}$ to the expansion coefficients by requiring that if additional virtual orbitals $\tilde{\phi}_a$ are added, the density does not change. This is the case if

$$\langle \tilde{\phi}_a | \hat{T} + v | \phi_i \rangle = \langle \tilde{\phi}_a | \hat{h}_0 + \sum_t \Delta b_t g_t(\mathbf{r}) | \phi_i \rangle = 0, \quad (17)$$

where $\hat{h}_0 = \hat{T} + v_{\text{nuc}}(\mathbf{r}) + v_{\text{Coul}}(\mathbf{r}) + v_0(\mathbf{r}) + \sum_t b_t^0 g_t(\mathbf{r})$. To consider all possible extensions of the orbital basis set, the additional virtual orbitals can be chosen as

$$\tilde{\phi}_{\mathbf{r}'}(\mathbf{r}) = \delta(\mathbf{r} - \mathbf{r}') - \sum_j \phi_j(\mathbf{r}') \phi_j(\mathbf{r}), \quad (18)$$

where $\delta(\mathbf{r} - \mathbf{r}')$ is the Dirac delta function (or in practical calculations, a ‘‘finite element’’ function centered at a point \mathbf{r}' of the numerical integration grid) and where the second term ensures that the functions $\tilde{\phi}_{\mathbf{r}'}(\mathbf{r})$ are orthogonal to the occupied orbitals ϕ_i .

If the matrix elements in Eq. (17) are not zero, the first-order change in the electron density upon introduction of these additional virtual orbitals can be approximated as [cf. Eq. (12)]

$$\Delta \rho(\mathbf{r}) \approx \sum_i \phi_i(\mathbf{r}) \langle \tilde{\phi}_{\mathbf{r}'} | \hat{T} + v | \phi_i \rangle, \quad (19)$$

where the orbital energy differences and the orthogonality correction in the additional virtual orbitals have been neglected. Therefore, to arrive at a potential for which the density changes as little as possible when the orbital basis set is enlarged, we require

$$\int w(\mathbf{r}') \left(\sum_i \phi_i(\mathbf{r}') \langle \tilde{\phi}_{\mathbf{r}'} | \hat{T} + v | \phi_i \rangle \right)^2 d^3 r' \rightarrow \min, \quad (20)$$

where we have introduced a weighting function $w(\mathbf{r}')$ that determines the relative importance of the additional virtual orbitals. Our choice for this weighting function will be discussed shortly. The form of Eq. (20) is chosen such that it is invariant under unitary transformations of the occupied orbitals (see Appendix B). Because of its ill-posed nature, the

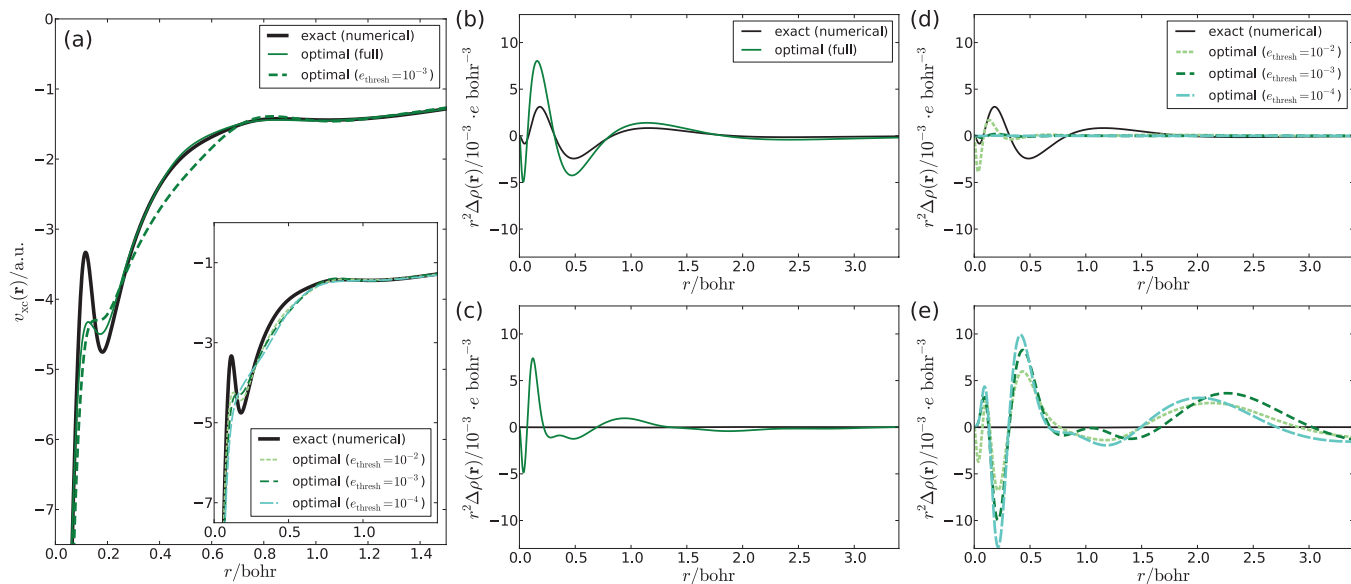


FIG. 2. (a): Exchange-correlation part $v_{xc}(\mathbf{r})$ of the optimal optimized potential for the argon atom and the target density from a calculation with the BP86 xc functional and a DZP basis set, compared to the corresponding exact reference (black solid line). The solid green line corresponds to the minimization of Eq. (20) without an additional constraint, whereas the dashed line is the optimal optimized potential obtained with the additional constraint that the density error in the finite basis set is below $e_{\text{thresh}} = 10^{-3} e \text{ bohr}^{-3}$. In the inset, different values of e_{thresh} are compared. All potentials have been shifted such that they match the exact potential at $r = 3.0 \text{ bohr}$. (b–e): Radial difference $r^2 \Delta \rho(\mathbf{r})$ between the target density and the density obtained from the different potentials. The difference densities in (b) and (c) refer to the potentials in part (a), whereas those in (d) and (e) are for the potentials shown in the inset. The upper plots (b) and (d) show the difference density in the finite basis set calculations and the lower plots (c) and (e) are for a numerical solution of the KS equations.

WY optimization performed in the first step can result in different potentials and different occupied orbitals yielding identical densities. However, these occupied orbitals usually only differ by a unitary transformation. The invariance of Eq. (20) under such transformations then ensures that the outcome of the minimization is the same. Therefore, the resulting potential is unambiguous.

After inserting the expansion of the potential given in Eq. (17), the minimization in Eq. (20) is again a standard quadratic optimization problem for the change in the expansion coefficients $\{\Delta \tilde{b}_t\}$. These can then be determined by solving a linear system of equations,

$$\mathbf{A} \Delta \mathbf{b} = -\mathbf{z}, \quad (21)$$

with

$$A_{st} = \sum_{ij} \int w(\mathbf{r}') \phi_i(\mathbf{r}') \phi_j(\mathbf{r}') \langle \tilde{\phi}_{r'} | \tilde{g}_s | \phi_i \rangle \langle \tilde{\phi}_{r'} | \tilde{g}_t | \phi_j \rangle d^3 r', \quad (22)$$

and the right hand-side

$$z_t = \sum_{ij} \int w(\mathbf{r}') \phi_i(\mathbf{r}') \phi_j(\mathbf{r}') \langle \tilde{\phi}_{r'} | \hat{h}_0 | \phi_i \rangle \langle \tilde{\phi}_{r'} | \tilde{g}_t | \phi_j \rangle d^3 r'. \quad (23)$$

The calculation of the integrals needed for setting up the matrix \mathbf{A} and the right-hand side \mathbf{z} is discussed in Appendix C.

If we solve this system of linear equations without a weighting function [i.e., with $w(\mathbf{r}) = 1$], it turns out that the resulting potential does not agree well with the exact reference potential because the minimization puts a too large weight on regions close to the nucleus where the electron density is very large. In addition, the matrix \mathbf{A} becomes ill-conditioned, as there are no strong conditions on more diffuse potential basis functions. Therefore, in order to obtain

a good overall description of the potential, it seems reasonable to choose the inverse density as a weighting function [i.e., $w(\mathbf{r}) = 1/\rho(\mathbf{r})$]. As will be shown, this results in optimized potentials that closely match the exact reference potential. Additional theoretical arguments for this choice of the weighting function are given in Appendices D and E. With this choice, the matrix \mathbf{A} becomes well-conditioned. Only if very diffuse functions are present in the potential basis set, \mathbf{A} has eigenvalues close to zero that are related to a constant shift of the potential.

The xc part of the optimized potential obtained from the minimization of Eq. (20) for the example of the argon atom is shown as green solid line in Fig. 2(a). We will refer to the potentials that have been obtained from the condition given in Eq. (20) as “optimal optimized potentials” in the following. It closely approximates the exact numerical reference, in particular for $r > 0.3$ and close to the nucleus. Moreover, it also recovers the shell structure of the exact potential, even though the feature at $r \approx 0.2$ is not as pronounced as in the reference potential. With this optimal potential, the density difference obtained when solving the KS equations numerically, shown as solid green line in Fig. 2(c), is also decreased significantly compared to all other reconstructed potentials and the absolute error in the density (see Table I) is reduced to $0.022 e \text{ bohr}^{-3}$. It is important to note that this close agreement between the optimal optimized potential and the numerical reference found with the small DZP orbital basis set does not contradict the theoretical analysis of Refs. 51 and 52 that showed that OEP methods require very large orbital basis sets. Here, a complete complementary basis set was introduced for the virtual orbital space for deriving Eq. (21).

We note that enlarging the basis set for the potential to the QZ4P-fit density fitting basis set does not change the re-

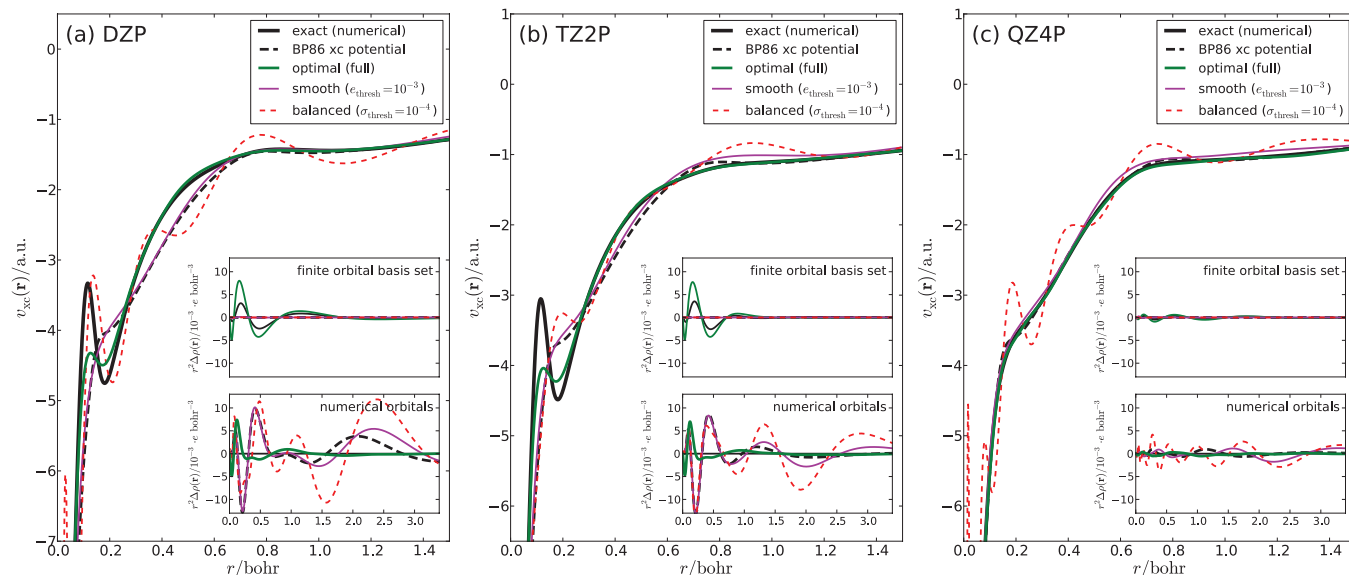


FIG. 3. Exchange-correlation part $v_{xc}(r)$ of the optimal optimized potential for the argon atom for target densities from a calculation with the BP86 xc functional and (a) the DZP basis set, (b) the TZ2P basis set, and (c) the QZ4P basis set. For comparison, the corresponding exact reference potentials (black solid line) and the potentials calculated as functional derivative of the BP86 xc energy functional (black dashed line) as well as the potentials obtained by requiring a smooth potential (magenta line) and with an implicitly balanced potential basis set (red dashed line) are also shown. All potentials are shifted such that they match the exact potential at $r = 3.0$ bohr. The insets show the radial difference $r^2 \Delta \rho(r)$ between the target density and the density obtained from the exact and the optimal optimized potentials. The upper inset refers to the density in the finite basis set calculations, whereas the lower inset is for a numerical solution of the KS equations.

sulting optimal optimized potential, i.e., our scheme makes it possible to go to the basis set limit for the expansion of the potential. The remaining differences between the exact reference potential and the optimized potential are caused by the finite orbital basis set, since the occupied orbitals obtained from the WY procedure differ from those in the exact numerical solution by more than a unitary transformation. Thus, by increasing the orbital basis set, the exact potential could be approached even more closely. This is demonstrated in Fig. 3, where the optimized exchange-correlation potentials for the argon atom are shown for orbital basis sets of increasing size. As target densities, the ground-state densities obtained with the BP86 exchange-correlation functional and the DZP, TZ2P, and QZ4P basis sets are used in Fig. 3(a)–3(c), respectively. To optimize the local potentials that yield these target densities, the same orbital basis set is used in combination with the corresponding density fitting basis set for expanding the potential.

When going from the DZP to the TZ2P orbital basis set, the exact reference potential and the optimized potential do not change significantly, but the absolute error obtained for comparing the density from the optimized potential to the target density is slightly reduced (see Table II). When the orbital basis set is further increased to QZ4P, the exact reference potential changes and the pronounced feature at $r \approx 0.2$ disappears. Since results close to the basis set limit can be obtained with such a basis set, the exact reference potential now agrees very well with the potential calculated as functional derivative of the BP86 exchange-correlation energy functional, shown as black dashed line in Fig. 3. However, the latter still has the wrong asymptotic form at larger distances from the nucleus. The optimal optimized potential now closely matches the exact reference potential. Moreover, the error in the density obtained from a numerical solution of the KS equations on the optimal optimized potential (see Table II) is further reduced to $0.011 e \text{ bohr}^{-3}$, and the corre-

TABLE II. Absolute error in the electron density compared to the target density (in $e \text{ bohr}^{-3}$) obtained with the exact reference potential, the potential calculated as functional derivative of the BP86 exchange-correlation functional, and the optimal optimized potential compared for different orbital basis sets. An argon atom and a target density from a BP86 calculation with the corresponding basis set is considered. The errors are given both for calculations with the finite orbital basis set ($e_{\text{dens}}^{\text{finite}}$) and for a numerical solution of the KS equations ($e_{\text{dens}}^{\text{numerical}}$).

	DZP		TZ2P		QZ4P	
	$e_{\text{dens}}^{\text{finite}}$	$e_{\text{dens}}^{\text{numerical}}$	$e_{\text{dens}}^{\text{finite}}$	$e_{\text{dens}}^{\text{numerical}}$	$e_{\text{dens}}^{\text{finite}}$	$e_{\text{dens}}^{\text{numerical}}$
Exact potential	0.025	$<10^{-4}$	0.018	$<10^{-4}$	0.007	$<10^{-4}$
BP86 xc potential	0.0	0.126	0.0	0.067	0.0	0.017
Balanced ($\sigma_{\text{thresh}} = 10^{-4}$)	$<10^{-4}$	0.306	$1.0 \cdot 10^{-4}$	0.189	$1.0 \cdot 10^{-4}$	0.086
Smooth ($\epsilon_{\text{thresh}} = 10^{-3}$)	$6.1 \cdot 10^{-4}$	0.166	$2.5 \cdot 10^{-4}$	0.104	$6.2 \cdot 10^{-4}$	0.043
Optimal (full)	0.054	0.029	0.037	0.023	0.011	0.011

sponding difference density (shown in the inset in Fig. 3(c)) almost vanishes.

For comparison, the smooth and implicitly balanced potentials obtained with thresholds of $e_{\text{thresh}} = 10^{-3}$ and $\sigma_{\text{thresh}} = 10^{-4}$ are also included in Fig. 3. For all three basis sets, the balanced potentials still show unphysical oscillations. These are removed when the smoothness constraint is applied. However, in this case the feature at $r \approx 0.2$, which is present with the DZP and TZ2P basis sets, is not reproduced. For the large QZ4P basis set, the smooth potential agrees well with both the optimal potential and with the numerical reference. However, these are still small deviations. These are revealed when the errors in the density obtained from a numerical calculation on the different optimized potentials (shown in the lower insets) and the corresponding density errors $e_{\text{dens}}^{\text{numerical}}$ (included in Table II) are considered. For all optimized potentials, this error decreases as the basis set is increased. However, for each basis set, the error is smallest for the optimal optimized potential. With the large QZ4P orbital basis set, it is four times larger for the smooth potential than for the optimal potential.

Returning to the optimal optimized potential obtained for the argon atom in the smaller DZP orbital basis set, shown in Fig. 2(a), another important observation is made. As shown in Fig. 2(b), it turns out that with the optimal optimized potential the density obtained in the finite orbital basis set does not agree with the target density anymore. As already mentioned earlier, this is also the case for the exact reference potential. Therefore, the requirements that the target density is (a) recovered in the finite orbital basis set and is (b) also recovered in a numerical calculation representing the basis set limit are not compatible with each other. For obtaining an optimized potential that closely matches the exact reference (i.e., fulfills the second requirement), the first requirement has to be sacrificed.

However, the discrepancy between these two requirements becomes smaller with increasing size of the orbital basis set. The upper parts of the insets in Fig. 3 show the difference between the densities obtained with the exact reference potential in finite orbital basis sets of increasing size and the target density, and the corresponding density errors are compared in Table II. The larger the orbital basis set, the smaller is the deviation from the target density. For the optimal optimized potentials, this difference decreases even faster.

For some applications, in particular in the context of embedding schemes, it might be necessary to require that the target density is reproduced also within the finite basis set. This can be achieved by including the constraint that in the finite orbital basis the absolute error in the density is below a threshold e_{thresh} in the minimization of Eq. (20). As described in Sec. V, this leads to a quadratic programming problem. Details on the employed algorithm for solving this problem are given in Appendix A. This way, one can obtain a potential that is a “compromise” between the two conflicting requirements. For $e_{\text{thresh}} = 10^{-3} e \cdot \text{bohr}^{-3}$, the resulting potential is included in Fig. 2(a) as green dashed line and the corresponding difference densities are shown in Fig. 2(d) and 2(e). This potential still matches the ex-

act potential closely but the difference between the density from a numerical calculation with this potential is larger than without the additional constraint. The optimized potentials obtained with thresholds of $e_{\text{thresh}} = 10^{-2} e \cdot \text{bohr}^{-3}$, $e_{\text{thresh}} = 10^{-3} e \cdot \text{bohr}^{-3}$, and $e_{\text{thresh}} = 10^{-4} e \cdot \text{bohr}^{-3}$ are compared in the inset of Fig. 2(a). As expected, the smaller this threshold is chosen, the larger is the deviation of the optimized potential from the exact reference.

VII. OPTIMAL OPTIMIZED POTENTIALS FOR ATOMS

To assess the performance of our scheme for determining the optimal optimized potential, we first consider additional tests for different atoms. In this case, it is possible to compare to the exact potentials, which can be obtained with the scheme of Ref. 20 in combination with a numerical solution of the KS equations. Instead of target densities from a local xc potential, we now consider target densities obtained from a Hartree–Fock (HF) calculation (i.e., from a non-local potential) in the small DZP basis set. For such small basis sets, the products of basis functions can be expected to be linearly independent. Therefore, reproducing the HF density with a local potential is equivalent to obtaining the same density matrix, and the HF energy is identical in both cases.^{15,52} However, this usually requires highly oscillating local potentials.¹⁵ With larger basis sets, products of basis functions become linearly dependent and different density matrices can yield the same electron density.⁵² Therefore, in a numerical calculation one can obtain a well-behaved local potential that reproduces the HF target density. However, the corresponding density matrices and HF energies will differ.⁵³

The exact local potentials that yield the target densities from a HF/DZP calculation for the beryllium atom, the neon atom, and the argon atom are shown in Fig. 4(a)–4(c) as black solid lines. The corresponding optimized potentials obtained from the WY scheme with implicitly balanced basis sets are included in this figure as red dashed line. In all three cases, this potential deviates considerably from the exact reference potentials. For the beryllium atom, it becomes positive close to the nucleus, whereas for neon and argon, unphysical oscillations appear. However, it is known that with small orbital basis sets, the HF densities can only be reproduced with such oscillating potentials.¹⁵ Therefore, singling out the optimized potential that is as smooth as possible [Eq. (15)] does only partly remove these differences (shown as magenta lines in Fig. 4). For beryllium, the smooth optimized potential is still wrong both close to the nucleus and also for neon and argon, one still observes rather large deviations from the numerical reference potential. Note that for the smooth and balanced potentials a larger threshold of $e_{\text{thresh}} = 10^{-2}$ and $\sigma_{\text{thresh}} = 10^{-2}$, respectively, was used here. If the same thresholds as for the BP86 target density (see Figs. 1 and 3) are used, these potentials show even larger oscillations.

The optimal optimized potential obtained from Eq. (20) without additional constraint are included in Fig. 4 as green solid lines. These potentials closely match the exact reference potentials, both close to the nucleus and at larger distances. The only differences are found in neon and argon for the feature at $r \approx 0.3$ and at $r \approx 0.2$, respectively. However, the op-

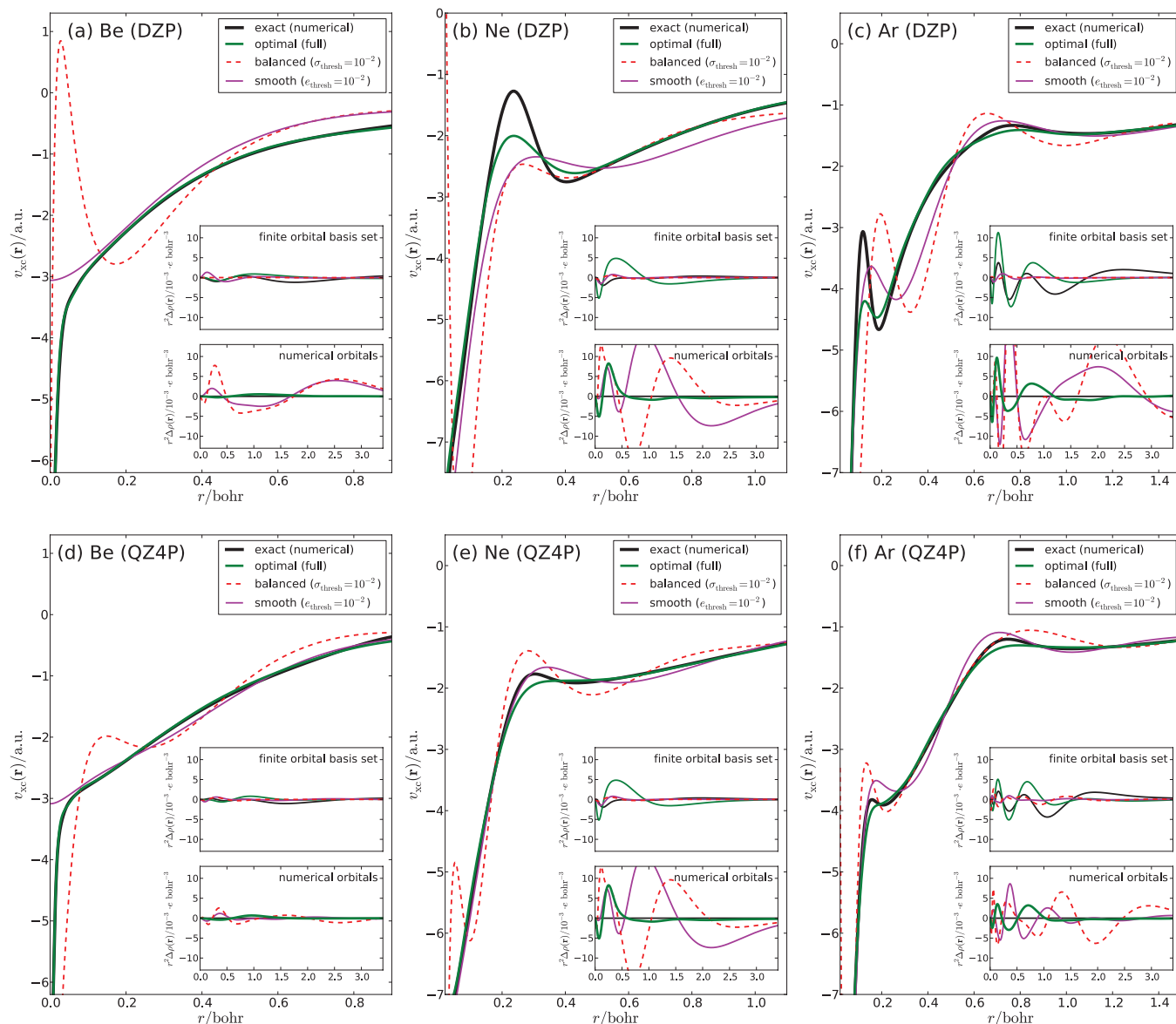


FIG. 4. Exchange-correlation part $v_{xc}(r)$ of the optimal optimized potential for (a,d) the beryllium atom, (b,e) the neon atom, and (c,f) the argon atom for target densities from a Hartree–Fock calculation with a DZP orbital basis set (upper row) and a QZ4P orbital basis set (lower row). For comparison, the corresponding exact reference potentials (black solid line) and the potentials obtained by requiring a smooth potential (magenta line) and with an implicitly balanced potential basis set (red dashed line) are also shown. All potentials are shifted such that they match the exact potential at $r = 3.0$ bohr. The insets show the radial difference $r^2\Delta\rho(r)$ between the target density and the density obtained from the exact reference and the different optimized potentials. The upper inset refers to the finite basis set calculations, whereas the lower inset is for a numerical solution of the KS equations.

timal optimized potentials still recover these features partly and show the correct shape in this region. This demonstrates that with our scheme it is possible to obtain an optimized potential that closely approximates the exact reference potential already with a rather small finite orbital basis set. The quality of the optimal optimized potentials can also be inferred from the comparison of the density obtained from these potentials in a numerical calculation with the target density, which is shown in the lower part of the insets in Fig. 4(a)–4(c). In all three cases, the differences are significantly smaller than for the optimized potential obtained with an implicitly balanced basis set or with the smooth optimized potential. Note, however, that within the finite orbital basis set the density from the optimal optimized potential differs from the target density.

With a very large orbital basis set, products of basis functions start to become linearly dependent. In this case, the HF density can be reproduced with well-behaved potentials. Therefore, the smooth and balanced potentials are closer to the numerical reference potential. This is shown in Fig. 4(d)–4(f) for the beryllium, neon, and argon atoms and a target density obtained from a HF calculation with the larger QZ4P basis set. However, even though the agreement is better than with the DZP orbital basis set, both the smooth and the balanced potentials still show significant deviations from the numerical reference potential. The balanced potentials still exhibit oscillations, in particular close to the nucleus, whereas the smooth potentials fail to reproduce the shell structure correctly. Moreover, for the beryllium atom the smooth potential

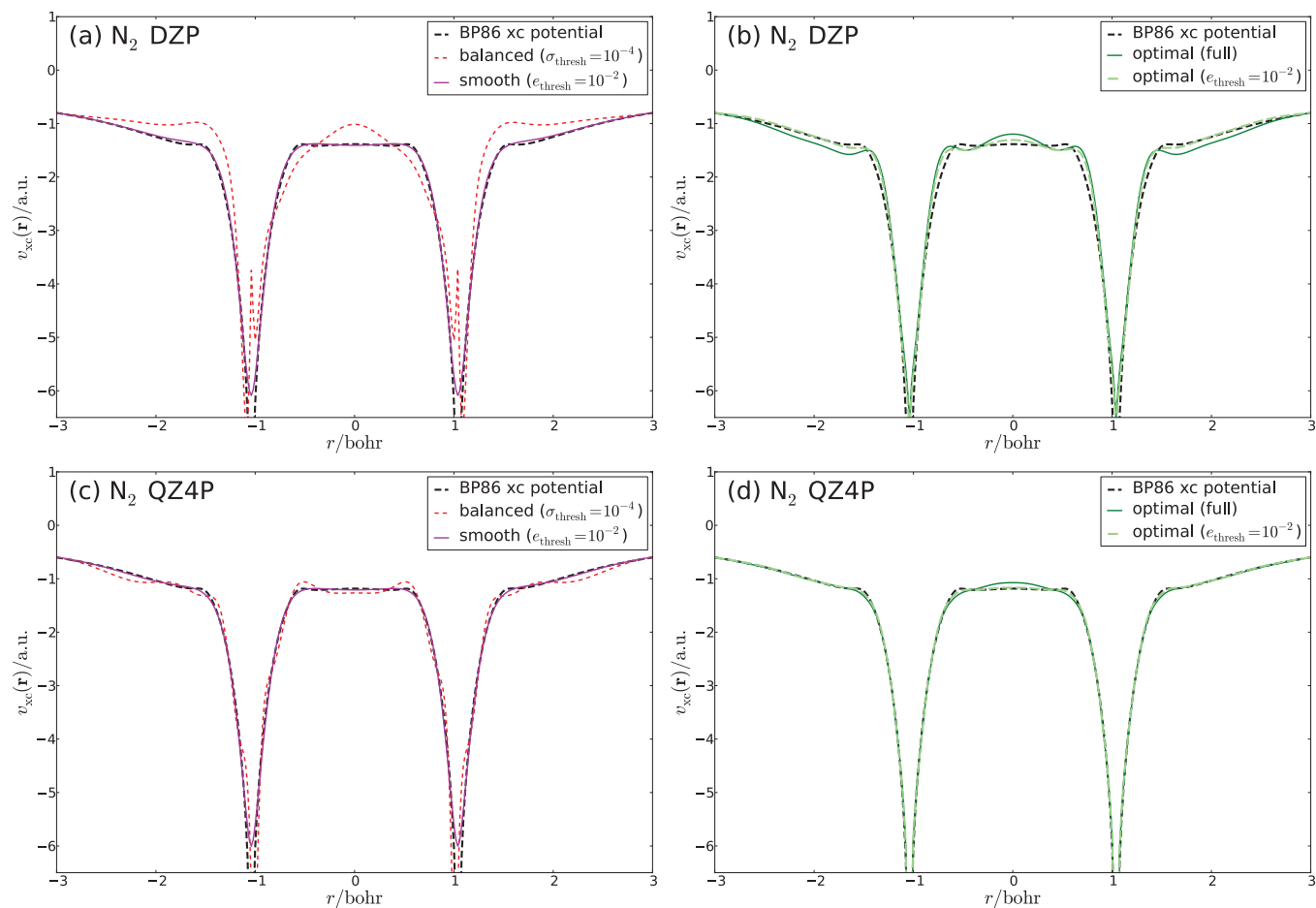


FIG. 5. Exchange-correlation part $v_{xc}(\mathbf{r})$ of the optimized potentials calculated with different schemes for an N_2 molecule along the bond axis. As target density, the ground-state density obtained with the BP86 xc functional in (a,b) a DZP orbital basis set and (c,d) a QZ4P orbital basis set is employed. The potential calculated from the target density as functional derivative of the BP86 xc energy functional is also included (black dashed line). All potentials have been shifted such that they match the BP86 xc potential at $r = -3.0$ bohr.

has a wrong behavior close to the nucleus. In contrast, the optimal optimized potentials closely match the numerical reference potential in all cases and only show small deviations in reproducing the feature at $r \approx 0.3$ and at $r \approx 0.2$ for neon and argon, respectively. In all cases, the density obtained from the optimal potentials with a numerical solution of the KS equations agrees best with the target density, as is shown in the lower part of the insets in Fig. 4(d)–4(f). Thus, both with the small DZP orbital basis set and with the larger QZ4P orbital basis set, the optimal optimized potential is superior to the potentials obtained with other approaches, even though the differences between all methods decrease as the orbital basis set increases. Note, however, that in order to obtain well-behaved smooth and balanced potentials rather large thresholds had to be used. With smaller thresholds, these potentials still show large unphysical oscillations in all cases.

VIII. OPTIMAL OPTIMIZED POTENTIALS FOR MOLECULES

Finally, we also performed tests of our scheme for simple molecules. However, in this case a comparison to the exact solution is not feasible anymore, because a fully numerical so-

lution of the KS equations would be required. To be able to assess the accuracy of the resulting optimized potentials, we first consider a target density obtained with a local potential. In Fig. 5, the exchange-correlation parts of the optimized potentials calculated for a target density from a BP86 calculation with a DZP and with a QZ4P basis set are shown. These can be compared to the potential calculated for the target density as functional derivative of the BP86 xc energy functional, i.e., the local potential that was used to calculate the target density. As discussed earlier for the example of the argon atom, this is one of the non-unique potentials that yield the target density in the finite orbital basis set. However, it is not the exact potential that yields the target density in the basis set limit. Nevertheless, except for the wrong asymptotic form the agreement with the exact potential should be rather good if a sufficiently large orbital basis set is used.

For the DZP target density (potentials shown in Fig. 5(a) and 5(b), the optimized potential obtained with an implicitly balanced basis set (red dashed line) shows oscillations close to the nuclei and has a different shape as the BP86 xc potential (black dashed line) in the bonding region and around $r \approx \pm 1.5$. Singling out the optimized potential that is as smooth as possible (magenta line) results in a potential that closely

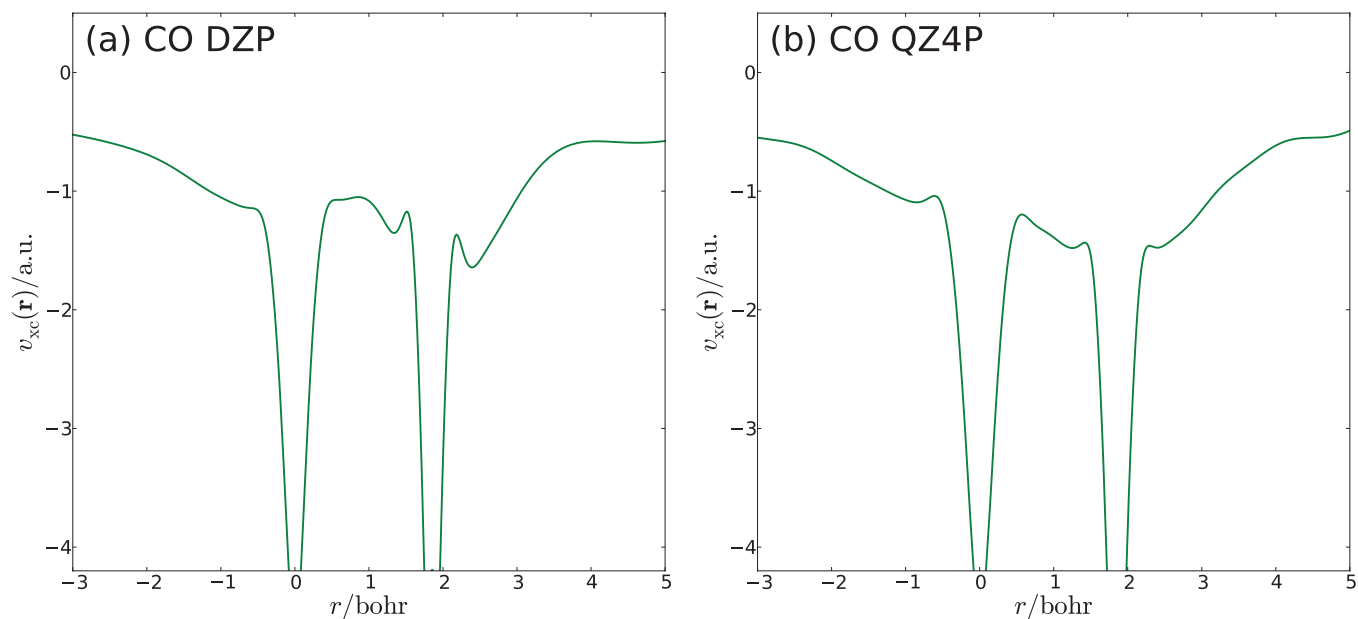


FIG. 6. Exchange-correlation part $v_{xc}(r)$ of the optimal optimized potentials for a CO molecule along the bond axis. As target density, the ground-state density obtained from a Hartree–Fock calculation in (a) a DZP orbital basis set and (b) a QZ4P orbital basis set is employed. For both basis sets, the corresponding smooth and balanced potentials show large unphysical oscillations and are, therefore, not shown.

matches the BP86 xc potential. The optimal optimized potential, shown as green line in Fig. 5(b), shows some additional features in the bonding region and around $r \approx \pm 1.5$. Note that for the example of the argon atom considered earlier, we found that with small basis sets such features are introduced in the exact potentials, which are correctly reproduced by the optimal optimized potential. Thus, it can be expected that these similar features in the optimal optimized potentials for the nitrogen molecule are indeed a correct approximation to the exact potential. By introducing an additional constraint on the deviation of the density in the finite basis set from the target density (green dashed line), these features are reduced and the potential approaches the BP86 potential more closely.

With the larger QZ4P orbital basis set, the difference between the BP86 xc potential and the exact potential should become smaller. We now find that the differences between the different optimized potentials (shown in Fig. 5(c) and 5(d)) further decreases. However, the potential obtained with an implicitly balanced basis set still shows smaller irregularities, such as for instance its asymmetric form around the nuclei, and deviates from the BP86 xc potentials. On the other hand, both the smooth optimized potential and the optimal optimized potential agree closely with the BP86 xc potential. Nevertheless, there are small differences between these two potentials, in particular close to the nuclei: while the smoothness constraint leads to a potential that has a finite value of approximately -6.0 a.u. at the nuclei, the optimal potential matches the BP86 xc potential more closely in this region and shows a steeper decrease as it approaches the nuclei.

As a another test case, we consider the CO molecule and use a target density from a Hartree–Fock calculations. As discussed in Sec. VII, such densities obtained from a nonlocal potential can only be reproduced in a finite basis set with

highly oscillating potentials.¹⁵ For this reason, both with an implicitly balanced basis set and when singling out the optimized potential that is as smooth as possible, highly oscillating potentials are obtained. In the latter case, a threshold as large as at least $0.1 e \text{ bohr}^{-1}$ is required to obtain a well-behaved potential. The optimal optimized potentials obtained for the Hartree–Fock target densities in a DZP and QZ4P orbital basis set are shown in Fig. 6(a) and 6(b). In both cases, well-behaved potentials are obtained that shown the same features as the exact-exchange (EXX) potential obtained in Ref. 17 with very large, uncontracted Gaussian-type orbital basis sets. Note, however, that these potentials correspond to a self-consistent EXX-OEP density close to the basis set limit, whereas we only considered finite basis set Hartree–Fock densities.

IX. CONCLUSIONS

With a finite orbital basis set, the optimization of effective potentials is an ill-posed problem. For developing a method that overcomes this obstacle, we have considered the special case of optimizing the local potential that yields a given target density in this work. This is equivalent to evaluating the functional derivative of the noninteracting kinetic energy and exhibits the same numerical problems as OEP schemes for evaluating orbital-dependent exchange-correlation functionals, such as EXX-OEP methods. In particular, highly oscillating and thus unphysical potentials can be obtained if the orbital and potential basis sets are not balanced.

To arrive at a method that can be applied for any combination of orbital and potential basis sets, one has to introduce a condition that singles out one unambiguous potential among those that yield almost identical densities. This leads to a

two-step procedure: first, a potential optimization algorithm is applied to obtain one non-unique potential that reproduces the target density as well as the associated occupied and virtual orbitals. Subsequently, an unambiguous optimized potential is determined in a second step. Here, the WY direct optimization algorithm has been used to obtain a non-unique potential in the first step. However, the approach presented here for singling out an unambiguous potential in the second step can also be combined with any other optimization method.

One possibility for setting up a condition to single out an unambiguous potential in the second step is to select the potential that is as smooth as possible, while still reproducing the target density up to a given threshold. But in many cases such a smooth optimized potential is not the desired solution, since the exact potential, i.e., the potential that yields the target density in the basis set limit, is not smooth. Therefore, we require that upon increasing the orbital basis set, the change in the electron density is minimized. The resulting approach for the optimization of effective potentials shows all the desired features of a generally applicable method. First, it does not require the use of balanced basis sets, and for any orbital basis set it is possible to increase the potential basis set until the basis set limit is reached. This is already possible for small orbital basis set, as was demonstrated for the DZP orbital basis set. Second, the resulting optimized potential is unambiguous. In particular, it does not depend on the (non-unique) outcome of the optimization in the first step and is, therefore, insensitive to its numerical details. Third, this optimal optimized potential closely approximates the exact potential already with rather small orbital basis sets, as has been shown in tests for atoms and molecules. In all test cases considered here, this optimal potential was closer to the reference potential than the optimized potentials obtained with a smoothness constraint or with implicitly balanced basis sets.

However, it turns out that the requirement that the optimal optimized potential yields the target density in the basis set limit is not compatible with the requirement that the target density is also reproduced in a smaller finite orbital basis set. Thus, in order to arrive at a potential that agrees as closely as possible with the exact solution, our scheme has to sacrifice the second requirement. If this is not acceptable, for instance when applying the optimized potentials within embedding schemes,^{30,31,33} this second requirement can be included as an additional constraint to arrive at a potential that is the best compromise. Moreover, if the size of the orbital basis set is increased, the discrepancy between the two requirements becomes smaller.

As a step towards EXX-OEP calculations, we have tested our approach for optimizing the potentials that yield target densities obtained from Hartree–Fock calculations. For atoms, the optimal optimized potentials from our approach can be shown to agree very well with the exact potential from a numerical calculation, whereas all other schemes give very different and often unphysical potentials. This is because these other schemes require that the target density is reproduced in the finite basis set, which is only possible with such unphysical potentials. On the other hand, our approach gives up this requirement in favor of reproducing the density as closely as possible in the basis set limit.

As a next step, the approach presented here can be extended to self-consistent EXX-OEP calculations and to the evaluation of the local xc potential for other orbital-dependent xc functionals. In such calculations, the local potential can be determined by minimizing an orbital-dependent functional with respect to the potential.¹¹ To make this minimization unambiguous with finite orbital basis sets, the optimization has to be constraint to include only those potentials that are—within the finite orbital basis set—related to a density by the constraint of Eq. (20). Such a constraint can be included both in a direct optimization¹² and in a self-consistent solution of the OEP equations.^{10,17} Work along these lines is currently in progress in our group.

ACKNOWLEDGMENTS

The author thanks Dr. Daniel Rohr for many inspiring discussions. Funding from the DFG-Center for Functional Nanostructures (CFN) at KIT is gratefully acknowledged.

APPENDIX A: TREATMENT OF THE INEQUALITY CONSTRAINTS ON $\{\Delta\tilde{b}_t\}$

In the absence of additional constraints, both the condition for obtaining a smooth potential [Eq. (15)] and for obtaining the optimal potential [Eq. (20)] are standard quadratic optimization problems, for which the minimum can be found by solving the linear system of equations [Eqs. (16) and (21), respectively],

$$A \Delta\tilde{\mathbf{b}} = -\mathbf{z}. \quad (\text{A1})$$

for the change $\{\Delta\tilde{b}_t\}$ in the expansion coefficients of the potential. Additional equality constraints could be introduced by the method of Lagrangian multipliers. If inequality constraints are introduced, one obtains a quadratic programming problem. Such problems and algorithms for solving them are, for instance, discussed in Ref. 50.

To ensure that the change in the electron density is below a chosen threshold, we have to introduce the inequality constraint [Eq. (14)],

$$4 \sum_t \sigma_t d_t |\Delta\tilde{b}_t| \leq e_{\text{thresh}}. \quad (\text{A2})$$

This is an inequality constraint on the absolute values of the change in the expansion coefficients $\{\Delta\tilde{b}_t\}$ with respect to the potential basis functions transformed with the right singular vectors of the matrix \mathbf{B} . We note that in the case of determining the optimal potential, Eq. (21) first has to be transformed in this way, i.e., in Eqs. (22) and (23), the potential basis functions $g_t(\mathbf{r})$ are replaced by the transformed potential basis functions $\tilde{g}_t(\mathbf{r})$.

Such an inequality constraint on the absolute values could be rewritten as 2^N normal inequality constraints (where N is the number of potential basis functions). However, a more tractable way of including such an absolute value constraint⁵⁴ is to express the coefficients as $\Delta\tilde{b}_t = \Delta\tilde{b}_t^+ - \Delta\tilde{b}_t^-$ with $\Delta\tilde{b}_t^+ \geq 0$ and $\Delta\tilde{b}_t^- \geq 0$. Then, the absolute value

constraint is

$$4 \sum_t \sigma_t d_t \Delta \tilde{b}_t^+ + 4 \sum_t \sigma_t d_t \Delta \tilde{b}_t^- \leq e_{\text{thresh}}. \quad (\text{A3})$$

Thus, one has to solve a quadratic programming problem with $2N$ variables and $2N + 1$ constraints. These constraints can be treated efficiently, since Eq. (A3) is an equality constraint (otherwise there would be no need to introduce the constraint at all), whereas the remaining $2N$ constraints are simple non-negativity constraints.

In our implementation, the active set algorithms as described in Ref. 50 is employed for solving the quadratic programming problem. However, as there are only non-negativity constraints, a simplified version of this algorithm is sufficient.

APPENDIX B: INVARIANCE OF EQ. (20) UNDER UNITARY TRANSFORMATIONS

If a unitary transformation U is applied to the occupied orbitals, i.e., $\tilde{\phi}_i(\mathbf{r}) = \sum_j U_{ij} \phi_j(\mathbf{r})$, the right-hand side of the minimization condition in Eq. (20) becomes

$$\begin{aligned} & \int w(\mathbf{r}') \left[\sum_i \tilde{\phi}_i(\mathbf{r}') \langle \tilde{\phi}_{r'} | \hat{T} + v | \tilde{\phi}_i \rangle \right]^2 d^3 r' \\ &= \int w(\mathbf{r}') \left[\sum_i \left(\sum_j U_{ij} \phi_j(\mathbf{r}') \right) \right. \\ & \quad \left. \times \left(\sum_k U_{ik} \langle \tilde{\phi}_{r'} | \hat{T} + v | \phi_k \rangle \right) \right]^2 d^3 r' \\ &= \int w(\mathbf{r}') \left[\sum_{jk} \underbrace{\left(\sum_i U_{ij} U_{ik} \right)}_{=\delta_{jk}} \phi_j(\mathbf{r}') \langle \tilde{\phi}_{r'} | \hat{T} + v | \phi_k \rangle \right]^2 d^3 r' \\ &= \int w(\mathbf{r}') \left[\sum_i \phi_i(\mathbf{r}') \langle \tilde{\phi}_{r'} | \hat{T} + v | \phi_i \rangle \right]^2 d^3 r', \quad (\text{B1}) \end{aligned}$$

and for the additional virtual orbitals [Eq. (18)], one obtains

$$\begin{aligned} \tilde{\phi}_{r'}(\mathbf{r}) &= \delta(\mathbf{r} - \mathbf{r}') - \sum_j \tilde{\phi}_j(\mathbf{r}') \tilde{\phi}_j(\mathbf{r}) \\ &= \delta(\mathbf{r} - \mathbf{r}') - \sum_j \left(\sum_k U_{jk} \phi_k(\mathbf{r}') \right) \left(\sum_l U_{jl} \phi_l(\mathbf{r}) \right) \\ &= \delta(\mathbf{r} - \mathbf{r}') - \sum_j \phi_j(\mathbf{r}') \phi_j(\mathbf{r}). \quad (\text{B2}) \end{aligned}$$

Therefore, the minimization of Eq. (20) is not affected by a unitary transformations of the occupied orbitals and the resulting potential is unambiguous.

APPENDIX C: CALCULATION OF THE MATRIX ELEMENTS IN EQ. (22) AND EQ. (23)

For setting up the matrix A [Eq. (22)] and \mathbf{r} [Eq. (23)], we have to calculate the matrix elements

$$\begin{aligned} \langle \tilde{\phi}_{r'} | g_s | \phi_i \rangle &= \int \left(\delta(\mathbf{r} - \mathbf{r}') - \sum_k \phi_k(\mathbf{r}') \phi_k(\mathbf{r}) \right) g_s(\mathbf{r}) \phi_i(\mathbf{r}) d^3 r \\ &= g_s(\mathbf{r}') \phi_i(\mathbf{r}') - \sum_k \langle \phi_k | g_s | \phi_i \rangle \phi_k(\mathbf{r}'), \quad (\text{C1}) \end{aligned}$$

and

$$\begin{aligned} \langle \tilde{\phi}_{r'} | \hat{h}_0 | \phi_i \rangle &= \int \left(\delta(\mathbf{r} - \mathbf{r}') - \sum_k \phi_k(\mathbf{r}') \phi_k(\mathbf{r}) \right) \hat{h}_0 \phi_i(\mathbf{r}) d^3 r \\ &= \left[\hat{h}_0 \phi_i(\mathbf{r}) \right]_{\mathbf{r}=\mathbf{r}'} - \sum_k \phi_k(\mathbf{r}') \langle \phi_k | \hat{h}_0 | \phi_i \rangle \\ &= \left[\hat{h}_0 \phi_i(\mathbf{r}) \right]_{\mathbf{r}=\mathbf{r}'} - \epsilon_i \phi_i(\mathbf{r}'), \quad (\text{C2}) \end{aligned}$$

with

$$\begin{aligned} \left[\hat{h}_0 \phi_i(\mathbf{r}) \right]_{\mathbf{r}=\mathbf{r}'} &= -\frac{1}{2} \Delta \phi_i(\mathbf{r}') + \left(v_{\text{nuc}}(\mathbf{r}') + v_{\text{Coul}}(\mathbf{r}') \right. \\ & \quad \left. + v_0(\mathbf{r}') + \sum_t b_t^0 g_t^0(\mathbf{r}') \right) \phi_i(\mathbf{r}'), \quad (\text{C3}) \end{aligned}$$

and where in the last line we have used that within the finite orbital basis set, the occupied orbitals ϕ_i are eigenfunctions of \hat{h}_0 with orbital energies ϵ_i .

The elements of the matrix A are then given by

$$\begin{aligned} A_{st} &= \sum_{ij} \int w(\mathbf{r}') \phi_i(\mathbf{r}') \left(g_s(\mathbf{r}') \phi_i(\mathbf{r}') \right. \\ & \quad \left. - \sum_k \langle \phi_k | g_s | \phi_i \rangle \phi_k(\mathbf{r}') \right) \phi_j(\mathbf{r}') \\ & \quad \times \left(g_t(\mathbf{r}') \phi_j(\mathbf{r}') - \sum_l \langle \phi_l | g_t | \phi_j \rangle \phi_l(\mathbf{r}') \right) d^3 r', \quad (\text{C4}) \end{aligned}$$

and the elements of the vector on the right-hand side are given by

$$\begin{aligned} z_t &= \sum_{ij} \int w(\mathbf{r}') \phi_i(\mathbf{r}') \left(\left[\hat{h}_0 \phi_i(\mathbf{r}) \right]_{\mathbf{r}=\mathbf{r}'} - \epsilon_i \phi_i(\mathbf{r}') \right) \phi_j(\mathbf{r}') \\ & \quad \times \left(g_t(\mathbf{r}') \phi_j(\mathbf{r}') - \sum_k \langle \phi_k | g_t | \phi_j \rangle \phi_k(\mathbf{r}') \right) d^3 r'. \quad (\text{C5}) \end{aligned}$$

In our implementation, all required integrals are evaluated using the accurate numerical integration grid of the ADF program.^{40,41}

APPENDIX D: OPTIMAL OPTIMIZED POTENTIAL IN THE CASE OF ONE ORBITAL

In the case of only one orbital $\phi_1(\mathbf{r}) = \sqrt{\rho(\mathbf{r})}$, the corresponding local potential can be calculated directly by inverting the KS equation for this orbital. The local potential is then given by

$$v_s(\mathbf{r}) = \frac{\Delta\phi_1(\mathbf{r}')}{2\phi_1(\mathbf{r}')} + \epsilon_1. \quad (\text{D1})$$

For only one orbital, the condition in Eq. (20) reduces to

$$\int w(\mathbf{r}') \left[\phi_1(\mathbf{r}') \langle \tilde{\phi}_{\mathbf{r}'} | \hat{T} + v | \phi_1 \rangle \right]^2 d^3 r' \rightarrow \min, \quad (\text{D2})$$

with

$$\tilde{\phi}_{\mathbf{r}'}(\mathbf{r}) = \delta(\mathbf{r} - \mathbf{r}') - \phi_1(\mathbf{r}')\phi_1(\mathbf{r}). \quad (\text{D3})$$

By inserting Eq. (D3) into Eq. (D2) and rearranging one obtains

$$\begin{aligned} & \int w(\mathbf{r}') \left[v(\mathbf{r}')\phi_i^2(\mathbf{r}) - \frac{1}{2}\phi_1(\mathbf{r}')\Delta\phi_1(\mathbf{r}') - \epsilon_1\phi_1^2(\mathbf{r}') \right]^2 d^3 r' \\ &= \int w(\mathbf{r}') \left[\phi_i^2(\mathbf{r}) \left(v(\mathbf{r}') - \frac{\Delta\phi_1(\mathbf{r}')}{2\phi_1(\mathbf{r}')} - \epsilon_1 \right) \right]^2 d^3 r' \rightarrow \min, \end{aligned} \quad (\text{D4})$$

and if the inverse density is chosen as weighting function, $w(\mathbf{r}') = \rho(\mathbf{r}')^{-1} = 1/\phi_1^2(\mathbf{r}')$, the minimization condition becomes

$$\int \rho(\mathbf{r}) \left[v(\mathbf{r}') - \left(\frac{\Delta\phi_1(\mathbf{r}')}{2\phi_1(\mathbf{r}')} + \epsilon_1 \right) \right]^2 d^3 r' \rightarrow \min. \quad (\text{D5})$$

The term in square brackets is the squared difference between $v(\mathbf{r}')$ and the exact potential. By integrating over the product of this difference and the density, the associated energy difference is minimized. This provides a theoretical justification for our choice of the weighting function.

APPENDIX E: KING-HANDY POTENTIAL

If the exact KS orbitals corresponding to the target density $\rho_0(\mathbf{r})$ would be known, the local potential yielding these orbitals could be calculated according to Eq. (D1) from any single KS orbital by inverting the corresponding KS equation. If the exact KS orbitals are not known, but some set of occupied orbitals corresponding to the target density, these can be used to obtain an approximation to the corresponding local potential as

$$\begin{aligned} v_{\text{KH}}(\mathbf{r}) &= \sum_i \frac{\phi_i^2(\mathbf{r})}{\rho(\mathbf{r})} \left[\frac{\Delta\phi_i(\mathbf{r})}{2\phi_i(\mathbf{r})} + \epsilon_i \right] \\ &= \frac{1}{\rho(\mathbf{r})} \sum_i \left[\frac{1}{2}\phi_i(\mathbf{r})\Delta\phi_i(\mathbf{r}) + \epsilon_i\phi_i^2(\mathbf{r}) \right], \end{aligned} \quad (\text{E1})$$

i.e., by averaging the potentials calculated for each of the occupied orbitals according to Eq. (D1) and weighting them at

every point in space with the contribution of the corresponding orbital to the electron density. This expression for the local potential corresponding to a given set of occupied orbitals was derived in a different way by King and Handy (KH) in Ref. 55. Note, however, that the resulting KH potential is not invariant under unitary transformations of the occupied orbitals. Therefore, calculating the KH potential from the non-unique occupied orbitals resulting from the WY optimization does not give an unambiguous optimized potential.

However, our optimal optimized potential obtained from the minimization of Eq. (18) can be considered as a generalization of the KH expression for the potential. After inserting the definition of the additional virtual orbitals [Eq. (18)] into the minimization condition of Eq. (20), one obtains

$$\begin{aligned} & \int w(\mathbf{r}') \left[\sum_i \phi_i(\mathbf{r}') \right. \\ & \quad \left. \times \sum_j \langle \delta(\mathbf{r} - \mathbf{r}') - \phi_j(\mathbf{r}')\phi_j(\mathbf{r}') | \hat{T} + v | \phi_i \rangle \right]^2 d^3 r' \\ & \rightarrow \min. \end{aligned} \quad (\text{E2})$$

If one now neglects all terms for which $i \neq j$, this condition turns into

$$\begin{aligned} & \int w(\mathbf{r}') \left[\sum_i \phi_i(\mathbf{r}') \left(-\frac{1}{2}\Delta\phi_i(\mathbf{r}') \right. \right. \\ & \quad \left. \left. + v(\mathbf{r}')\phi_i(\mathbf{r}') - \epsilon_i\phi_i(\mathbf{r}') \right) \right]^2 d^3 r' = \int w(\mathbf{r}') \left[\sum_i \phi_i^2(\mathbf{r}')v(\mathbf{r}') \right. \\ & \quad \left. - w(\mathbf{r}') \sum_i \left(\frac{1}{2}\phi_i(\mathbf{r}')\Delta\phi_i(\mathbf{r}') + \epsilon_i\phi_i^2(\mathbf{r}') \right) \right]^2 d^3 r' \rightarrow \min. \end{aligned} \quad (\text{E3})$$

When choosing the inverse density as weighting function, i.e., for $w(\mathbf{r}') = 1/\sum_i \phi_i^2(\mathbf{r}')$, this reduces to

$$\int \rho(\mathbf{r}) \left(v(\mathbf{r}') - v_{\text{KH}}(\mathbf{r}') \right)^2 d^3 r' \rightarrow \min, \quad (\text{E4})$$

i.e., $v(\mathbf{r})$ is determined such that the energy difference associated with the squared difference between $v(\mathbf{r})$ and the KH potential is minimized. This provides an additional justification for our choice of the weighting function. It is important to note that the additional terms with $i \neq j$ in Eq. (E2) ensure that our minimization condition is invariant under unitary transformations of the occupied orbitals, which is not the case for the KH potential.

¹W. Kohn and L. J. Sham, *Phys. Rev.* **140**, A1133 (1965).

²R. G. Parr and W. Yang, *Density-Functional Theory of Atoms and Molecules* (Oxford University Press, Oxford, 1989).

³J. P. Perdew and K. Schmidt, in *Density Functional Theory and Its Application to Materials*, edited by V. Van Doren, C. van Alsenoy, and P. Geerlings (AIP, Melville, New York, 2001), pp. 1–20.

⁴A. J. Cohen, P. Mori-Sanchez, and W. Yang, *Science* **321**, 792 (2008).

⁵E. J. Baerends and O. V. Gritsenko, *J. Chem. Phys.* **123**, 062202 (2005).

⁶J. Tao, J. P. Perdew, V. N. Staroverov, and G. E. Scuseria, *Phys. Rev. Lett.* **91**, 146401 (2003).

- ⁷J. Heyd, G. E. Scuseria, and M. Ernzerhof, *J. Chem. Phys.* **118**, 8207 (2003).
- ⁸F. Furche, *J. Chem. Phys.* **129**, 114105 (2008).
- ⁹J. D. Talman and W. F. Shadwick, *Phys. Rev. A* **14**, 36 (1976).
- ¹⁰A. Görling, *Phys. Rev. A* **46**, 3753 (1992).
- ¹¹W. Yang and Q. Wu, *Phys. Rev. Lett.* **89**, 143002 (2002).
- ¹²Q. Wu and W. Yang, *J. Chem. Phys.* **118**, 2498 (2003).
- ¹³F. Jensen, *Introduction to Computational Chemistry*, 2nd ed. (Wiley, Chichester, 2007).
- ¹⁴W. Koch and M. C. Holthausen, *A Chemist's Guide to Density Functional Theory*, 2nd ed. (Wiley-VCH, Weinheim, 2001).
- ¹⁵V. N. Staroverov, G. E. Scuseria, and E. R. Davidson, *J. Chem. Phys.* **124**, 141103 (2006).
- ¹⁶T. Heaton-Burgess, F. A. Bulat, and W. Yang, *Phys. Rev. Lett.* **98**, 256401 (2007).
- ¹⁷A. Heßelmann, A. W. Götz, F. Della Sala, and A. Görling, *J. Chem. Phys.* **127**, 054102 (2007).
- ¹⁸F. A. Bulat, T. Heaton-Burgess, A. J. Cohen, and W. Yang, *J. Chem. Phys.* **127**, 174101 (2007).
- ¹⁹Q. Zhao, R. C. Morrison, and R. G. Parr, *Phys. Rev. A* **50**, 2138 (1994).
- ²⁰R. van Leeuwen and E. J. Baerends, *Phys. Rev. A* **49**, 2421 (1994).
- ²¹F. Colonna and A. Savin, *J. Chem. Phys.* **110**, 2828 (1999).
- ²²T. W. Keal and D. J. Tozer, *J. Chem. Phys.* **119**, 3015 (2003).
- ²³T. W. Keal and D. J. Tozer, *J. Chem. Phys.* **121**, 5654 (2004).
- ²⁴M. J. G. Peach, A. M. Teale, and D. J. Tozer, *J. Chem. Phys.* **126**, 244104 (2007).
- ²⁵M. J. G. Peach, A. M. Miller, A. M. Teale, and D. J. Tozer, *J. Chem. Phys.* **129**, 064105 (2008).
- ²⁶A. M. Teale, S. Coriani, and T. Helgaker, *J. Chem. Phys.* **130**, 104111 (2009).
- ²⁷A. M. Teale, S. Coriani, and T. Helgaker, *J. Chem. Phys.* **132**, 164115 (2010).
- ²⁸G. Senatore and K. R. Subbaswamy, *Phys. Rev. B* **34**, 5754 (1986).
- ²⁹P. Cortona, *Phys. Rev. B* **46**, 2008 (1992).
- ³⁰S. Fux, Ch. R. Jacob, J. Neugebauer, L. Visscher, and M. Reiher, *J. Chem. Phys.* **132**, 164101 (2010).
- ³¹J. D. Goodpaster, N. Ananth, F. R. Manby, and T. F. Miller, *J. Chem. Phys.* **133**, 084103 (2010).
- ³²J. D. Goodpaster, T. A. Barnes, and T. F. Miller, *J. Chem. Phys.* **134**, 164108 (2011).
- ³³O. Roncero, M. P. de Lara-Castells, P. Villarreal, F. Flores, J. Ortega, M. Paniagua, and A. Aguado, *J. Chem. Phys.* **129**, 184104 (2008).
- ³⁴O. Roncero, A. Zanchet, P. Villarreal, and A. Aguado, *J. Chem. Phys.* **131**, 234110 (2009).
- ³⁵C. Huang, M. Pavone, and E. A. Carter, *J. Chem. Phys.* **134**, 154110 (2011).
- ³⁶S. Liu and P. W. Ayers, *Phys. Rev. A* **70**, 022501 (2004).
- ³⁷Y. Wang and R. G. Parr, *Phys. Rev. A* **47**, R1591 (1993).
- ³⁸E. S. Kadantsev and M. J. Stott, *Phys. Rev. A* **69**, 012502 (2004).
- ³⁹P. Mori-Sanchez, Q. Wu, and W. Yang, *J. Chem. Phys.* **123**, 062204 (2005).
- ⁴⁰Theoretical Chemistry, Vrije Universiteit Amsterdam, "ADF, Amsterdam density functional program," see <http://www.scm.com>.
- ⁴¹G. te Velde, F. M. Bickelhaupt, E. J. Baerends, C. Fonseca Guerra, S. J. A. van Gisbergen, J. G. Snijders, and T. Ziegler, *J. Comput. Chem.* **22**, 931 (2001).
- ⁴²Ch. R. Jacob, S. M. Beyhan, R. E. Bulo, A. S. P. Gomes, A. W. Götz, K. Kiewisch, J. Sikkema, and L. Visscher, *J. Comput. Chem.* **32**, 2328 (2011).
- ⁴³D. Andrae and J. Hinze, *Int. J. Quantum Chem.* **63**, 65 (1997).
- ⁴⁴G. Eickerling and M. Reiher, *J. Chem. Theory Comput.* **4**, 286 (2008).
- ⁴⁵A. D. Becke, *Phys. Rev. A* **38**, 3098 (1988); J. P. Perdew, *Phys. Rev. B* **33**, 8822 (1986).
- ⁴⁶Q. Wu, P. W. Ayers, and W. Yang, *J. Chem. Phys.* **119**, 2978 (2003).
- ⁴⁷S. Hirata, S. Ivanov, I. Grabowski, R. J. Bartlett, K. Burke, and J. D. Talman, *J. Chem. Phys.* **115**, 1635 (2001).
- ⁴⁸C. Kollmar and M. Filatov, *J. Chem. Phys.* **127**, 114104 (2007).
- ⁴⁹T. Heaton-Burgess and W. Yang, *J. Chem. Phys.* **129**, 194102 (2008).
- ⁵⁰J. Nocedal and S. Wright, *Numerical Optimization*, 2nd ed. (Springer, New York, 2006).
- ⁵¹A. Görling, A. Heßelmann, M. Jones, and M. Levy, *J. Chem. Phys.* **128**, 104104 (2008).
- ⁵²A. Heßelmann and A. Görling, *Chem. Phys. Lett.* **455**, 110 (2008).
- ⁵³S. Ivanov and M. Levy, *J. Chem. Phys.* **119**, 7087 (2003).
- ⁵⁴R. Tibshirani, *J. R. Stat. Soc. Ser. B (Methodol.)* **58**, 267 (1996).
- ⁵⁵R. A. King and N. C. Handy, *Phys. Chem. Chem. Phys.* **2**, 5049 (2000).